ISIJ International, Vol. 57 (2017), No. 1, pp. 1–14

Review

Twin Roll Casting of Steels: An Overview

Ali MALEKI,[1)]* Aboozar TAHERIZADEH[1,2)] and Nazanin HOSSEINI[1)]

1) Research Institute for Steel, Isfahan University of Technology, Isfahan, 8415683111 Iran.
2) Department of Materials Engineering, Isfahan University of Technology, Isfahan, 8415683111 Iran.

(*Received on August 16, 2016; accepted on September 20, 2016*)

The idea of twin-roll casting (TRC) was first patented by Sir Henry Bessemer in 1857. Development of the TRC process took more than 100 years and now it is commercialized for production of both ferrous and non-ferrous alloys particularly for some special steels. The process has significantly lower energy consumption and pollution compared to conventional processes and some other benefits as well as some limitations. This overview explains the history and principles of TRC for steels. Moreover, the utilization of TRC for different categories of steels and the following microstructural and mechanical properties is discussed in details.

KEY WORDS: twin-roll casting (TRC); steel; continuous casting; microstructure.

1. Introduction

Direct strip casting (DSC) is an emerging technology in the steel industry,[1,2)] which produces thin steel strips in a thickness range of 2–6 mm directly from liquid steel.[3–5)] As thickness of the as-cast strip is approximately close to the final product thickness, there is the possibility of eliminating the expensive and energy-consuming downstream rolling and finishing steps which are necessary in conventional continuous casting (CCC) and thin-slab casting (TSC). Using DSC technique, casting and rolling steps are merged into a single compact, efficient and continuous operation step resulting in many economic, environmental and technical benefits in the steelmaking industries.[5)] Unlike conventional slab casting, strip casting is carried out without mould flux, results in direct contact between the liquid steel and the mould surface, and consequently much higher heat fluxes and solidification rates.[6)] The high solidification rates achieved during strip casting have beneficial effects on the microstructure including high solubility in solid state, fine grain size, reduced microsegregation and dendrite arm space, and smaller inclusion size.[7)] The crystallographic texture of as-cast steel strips and its through-thickness texture gradient is weak. This is responsible for a more isotropic behavior compared to hot-rolled sheets.[8)] As well, it is advantageous for strength and deep drawing properties of the final sheets.[8,9)] Additionally, the production of small quantity of highly alloyed stainless steels by CCC and subsequent hot-rolling is not economical. In fact, DSC is recently introduced as a competitive method for the production of stainless steels[5)] and low carbon steels sheets.[10)] In this paper, the DSC and its advantages compared to CCC and TSC has been overviewed. Moreover, principles of TRC for steels and its application for different grades of steels have been explained.

2. Overview of Strip Casting

Steel strips with thicknesses in order of millimeters are standard products of the steel industry. Over the past decades, a lot of efforts have been devoted to develop hot strip production processes with high efficiency and productivity. Before the 1960's, ingot casting was used to produce steel strips. In this process, molten steel was cast into large steel moulds as ingots. It was then followed by transportation of ingots to a breakdown mill where they were reheated and processed into slabs with a thickness of 200–300 mm using a roughing mill.[11)] The invention of CCC process in 1952 and its implementation in 1970's enabled industries to convert directly the molten steel into semi-finished products (slabs, billet and blooms) with thickness range of 200–300 mm. These semi-finished products were then reheated and rolled into strip of 1–10 mm final thickness. It should be noted that the elimination of breakdown mill step significantly reduced the costs of CCC process compared to ingot casting.[2)] In 1989, the TSC process was invented and slabs of 50–60 mm thick were cast directly from the melt. Casting and hot-rolling were integrated into one continuous process, where thin slabs were subsequently passed into a reheating furnace directly and then hot-rolled in-line, into strips with a thickness of 1–10 mm. Consequently, the cost of reheating and rolling was considerably reduced.[11)] Whereas, strip casting technology, the most recent casting technology, integrates casting and rolling and makes the direct casting of steel slabs with a thickness of 1–5 mm possible.[2,3)] Thus, the process chain can be considerably shortened, which has a significant effect on the production costs.[5)] The evolution of hot strip production technology is summarized in **Fig. 1**.

* Corresponding author: E-mail: maleki110@cc.iut.ac.ir
DOI: http://dx.doi.org/10.2355/isijinternational.ISIJINT-2016-502

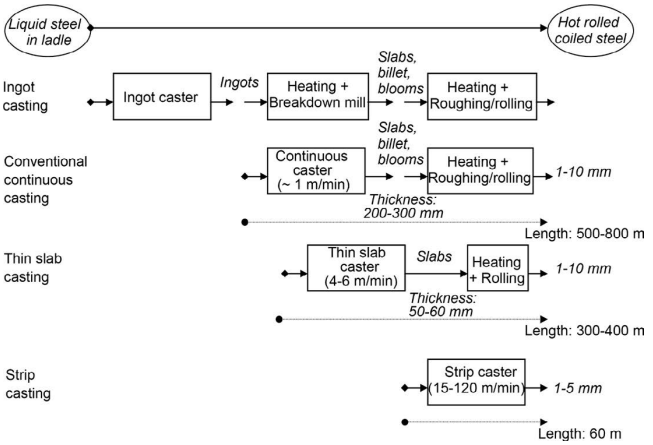

Fig. 1. Evolution of hot steel strip production technology: ingot casting, CCC, TSC and strip casting technology.[2)]

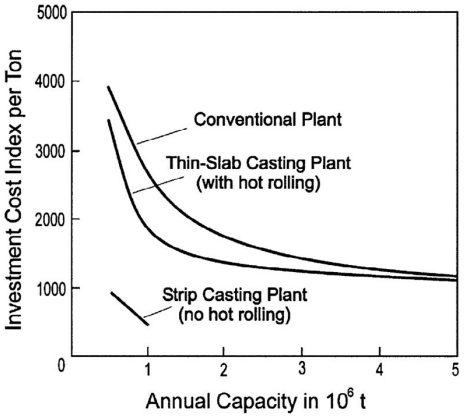

Fig. 2. Comparison of typical investment cost and annual capacity for various steel continuous casting routes.[14)]

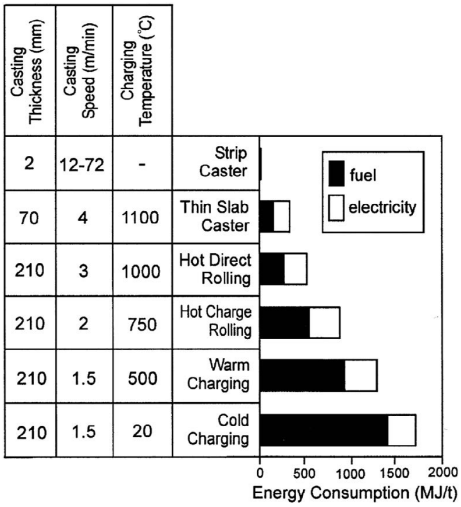

Fig. 3. Energy consumption associated with various casting processes of steel.[15)]

3. Advantages of DSC

The cost of strip production increases significantly as the final product thickness decreases and the initial slab thickness increases.[12)] In the process of TSC, the production costs start to increase dramatically if the strip is milled to a thickness less than 1.2 mm. It is worthy to note that DSC process allows strip to be produced at a thickness less than 1.8 mm at a stable cost.[13)]

3.1. Economic Benefit

After completion of steelmaking, application of DSC allows elimination of all flat steel products milling steps except some cold rolling mills and a few finishing operations.[13)] To achieve full economic benefits of DSC and, hence, compete with other continuous casting processes, it is necessary to consider costs of initial investment, operation, maintenance, and energy consumption.

Figure 2 exhibits the relationship between initial investment cost and annual capacity of flat steel products using various CCC, TSC and DSC. It indicates that for production of 1 Mt p.a. steel strip, the investment cost for a DSC plant is respectively a quarter and one fifth of that required for a TSC and CCC plant.[14)] It is noticeable that DSC process is cost benefit only for small plants while for large scale plants CCC or TSC is more appropriate.

The accurate calculations of the production costs also depend on the steel grade and its final application. As for stainless steel, it is anticipated that one ton of steel is 50 to 150 USD cheaper in the case of DSC compared to that of the TSC. Money also could be saved due to lower transportation costs.[13)]

3.2. Energy and Environmental Benefits

Apart from economic savings, the DSC technique is more energy efficient and has less environmental impact. The energy consumption associated with various steel manufacturing processes is depicted in **Fig. 3** emphasizing the significant reduction of energy consumption for DSC compared to TSC and conventional slab casting.[15)] In addition, the DSC process is an environment friendly process since it utilizes up to 90% less energy to process liquid steel directly into sheet form and reduces greenhouse gas emissions by up to 80% compared with CCC and secondary processing.[16)]

An additional environmental impact associated with DSC is the ability to make better use of scrap and recycled products. There is, however, some debate concerning the availability of adequate quality recycled steel scrap to achieve the full environmental benefits of DSC.[17)] As stated before, DSC generates higher solidification rates in comparison with CCC and TSC leading to reduction of microsegregation in steel strips. Consequently, alloy cleanliness requirements may not be so critical and lower quality scrap, usually inappropriate for CCC of steel strips, can be used in the DSC process.[14)]

The elimination of several intermediate reheating operations and shorter reheating times during DSC allows a reduction in deleterious gas emissions per ton of cast steel: CO_2 by ~ 7 times (from 185 to 25 kg), NO_x by 15 times (from 290 to 10 g) and SO_2 by 3 times (from 50 to 15 g). As a result, application of the strip casting technology allows a reduction in the total volume of deleterious emissions such as CO_2, SO_2 and NO_x between 70 and 90% in comparison with the conventional processes.[13)]

4. Types of Strip Caster

Hendricks *et al.*[18)] proposed an extended classification

scheme in 1995 by which the strip casters were divided into three major groups. **Figure 4** summarizes schematically some of the major technological groups in DSC involving moving moulds. Group I (Fig. 4(a)) are the Belt Casters (BC's) which uses water cooled travelling moulds or conveyor belts. Liquid steel is cast directly onto a belt (i), or sprayed (ii), or cast between two belts either inclined (iii) or vertical (iv). Group II (Fig. 4(b)) uses a single-roll caster (SRC) to produce thin-gauge strip. Two different feed systems are typically used, melt-spinning and melt-drag. In the single-roll process, the strip is made by dragging the liquid melt in contact with the rotating wheel due the momentum of the wheel and the surface tension of the liquid. Group III comprises the TRC of various configurations: vertical (i), horizontal 2-high (ii), horizontal 4-high (iii), inclined (iv), and asymmetrical twin rolls (v).

Generally, there have been several R&D projects for single-roll strip casters for steel, but they were eventually abandoned, either because of technical difficulties, or in favour of the other designs such as TRC.[3] It should be mentioned that TRC of steels is mainly focused on vertical casting technology.[14]

5. Twin-roll Casting

In 1857, Sir Henry Bessemer, a well-known steelmaker, developed a simple twin-roll casting setup using two hardened rolls and a small nine kilogram-capacity crucible, as shown in **Fig. 5**(a). Later, in 1865 he patented the strip casting of steel and iron, as illustrated in Fig. 5(b).[3,13] Generally, TRC utilizes two counter-rotating rolls to form two individual shells that are formed into a continuous sheet at the roll nip.[19] However, Bessemer faced with a lot of obstacles in the field of TRC of steel strip due to the thermal-physical properties of as-cast strip,[13,14] complicated control of fluid flow and metal distribution between the rolls, refractory problems in the "pour box", edge containment and poor surface quality.[14] Additionally, large production capacity was required to make the process profitable. Consequently, despite enormous efforts by researchers, the TRC of steel strip has only recently become feasible.[13]

5.1. Principles of Twin-roll Casting of Steels

Unlike TRC of aluminium sheet, the development of this process in the steel industry was terminated in the 1940's due to difficulties with roll wear, low productivity, poor as-cast strip quality, and variable solidification structure and mechanical properties.[13,20,21] Responsible factors for the delay in commercializing TRC of steel included the high melting point and density, the complexity of the Fe–Fe_3C phase diagram and low thermal conductivity compared with aluminium. Consequently, significant engineering advances in DSC were essential before the Bessemer's idea could be commercialized. During the last two decades, an extensive research and development program in the area of TRC of steels is carried out to: (i) generate a better understanding of early solidification; (ii) develop procedures for uniform delivery of molten metal; (iii) devise methods for controlling the melt pool edge; (iv) control roll distortion, and (v) understand the interactions between molten steel and refractory materials. In March 2000, the US steel company, Nucor, joined BHP (Australian steel company) and IHI Japanese plant manufacture to establish Castrip Limited Liability Company (Castrip LLC) as the first license of the TRC technology. A schematic diagram of the Castrip LLC plant setup is illustrated in **Fig. 6**. Although, the initial thickness of sheet produced by Castrip was around 1.7–1.8 mm, this process exhibited the capability of casting sub-millimeter gauge strip. Figure 6 demonstrates an in-line rolling mill generating a further reduction of 15–30% in strip thickness. In 2005, Castrip had the capability of producing over 500 000 Mt p.a. of strip-cast steel in a range of grades for various markets.[14]

The steel strip formation via TRC is an extremely fast process in which solidification time of the outer shell with a thickness of ~ 0.2 mm is in the order of ~ 0.02 s. The complete solidification of the steel strip takes place in less than a second.[14] The roll sleeve material for TRC of steels is mainly high conductivity copper alloy. To control the heat

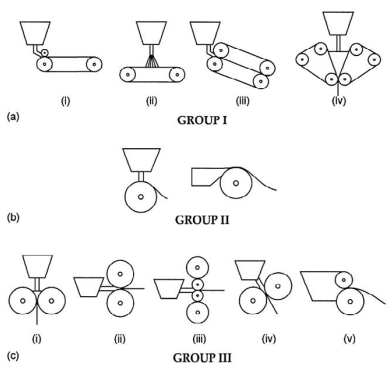

Fig. 4. Possible classification scheme for DSC.[18]

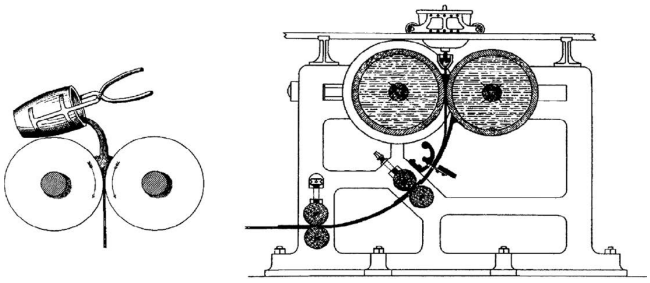

Fig. 5. (a) Bessemer's twin-roll caster design conceived in 1846 and patented in 1857 and (b) a twin-roll caster for steel, patented in 1865.[3]

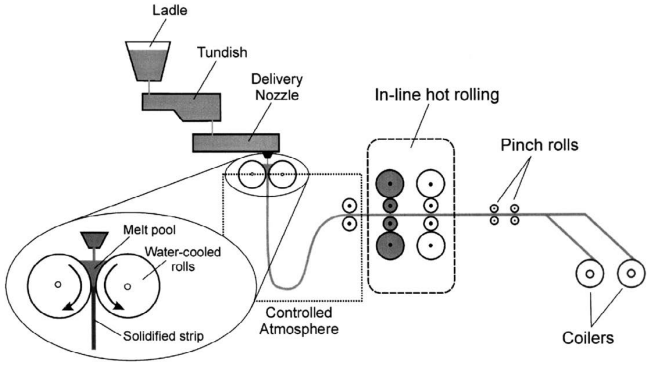

Fig. 6. A schematic diagram of the twin-roll strip casting process at Castrip LLC plant.[16]

transfer during casting, the roll surface may be textured. Roll surface texturing is achieved by a range of methods such as knurling, chemical etching, electric discharge machining, and laser ablation or shot blasting.[22] Moreover, the nozzle is made by a thermally resistant ceramic material such as alumina-graphite refractory.[14]

5.1.1. Twin-roll Casting of Low Carbon Steels

5.1.1.1. Effect of Titanium on TRC Strip

Girgensohn *et al.*[23] studied the properties of three different low carbon (LC) steels in various processing stages during twin-roll casting route using a laboratory twin-roll machine. **Table 1** indicates the chemical composition of investigated steels in this research. The first is a typical low carbon (LC) (aluminium killed) drawing steel. Titanium has been added to the second steel, which is also higher in carbon. The third one represents a commercial high strength low alloy (HSLA) grade.

Some surface defects such as triangles, beads, bleeds, edge defects, depressions and surface cracks occurs during twin-roll casting of LC steels. **Figure 7** illustrates the mentioned defects in LC steel strip. Triangles are formed when steel solidifies on the side dams. This defect is observed as a laminated patch on the strip surface. Additionally, triangles occur on both sides of the strip at irregular intervals of ~ 1–3 m. The lateral liquid steel leakage causes formation of bead defects, while the leakage on the strip surface results in bleed defects. Moreover, insufficient sealing between the rolls and side containment causes edge defects. It should be noted that depressions happen as a result of non-uniform contact and heat transfer between strip/roll, and subsequent uneven solidification.

Table 2 lists the possibility of defects occurrence during twin-roll casting of three categories of steels. As given in Table 2, the LC steel suffers from all defects in the list. The HSLA steel is much more easily cast in terms of all kinds of defects in the list. By addition of only 0.088 wt.% Ti to LC steel, the strip casting behavior of steel significantly was improved compared to the ordinary LC steel (see Table 2). **Figure 8** shows that the material with titanium addition is almost free of casting defects.

Microstructures of as-cast LC, LC+Ti and HSLA steel strips are shown in **Fig. 9**. As illustrated in Fig. 9(a), the as-cast LC steel strip contains large and irregular ferrite grains with the average grain size of ~ 60 μm indicating no sign of pearlite or carbide phases. This ferrite microstructure is also known as Widmanstatten or acicular ferrite. Coarse austenite grains and high cooling rates in the ferrite formation zone are the main reasons to obtain the mentioned microstructure.[23,24] By adding a small amount of Ti (0.088 wt.%), the average grain size of irregular ferrite decreases to ~ 25 μm (Fig. 9(b)) and some signs of dark pearlite grains become visible. Additionally, carbides are present, both at the grain boundaries and within grains. As for as-cast HSLA steel strip (Fig. 9(c)), the microstructure consists of fine grained bainite with some pearlite and carbide.

Figure 10 shows the microstructure of LC+Ti steel strip after in-line hot-rolling. According to this figure, the micro-

Table 1. Chemical compositions of steels (wt.%); O and N in ppm; S and P were always ≤ 0.003 wt.%.[23]

	C	Si	Mn	Al	Nb	Ti	N	O	Fe
LC	0.010	0.007	0.24	0.037	…	…	208	128	Bal.
LC+Ti	0.053	0.01	0.26	0.053	…	0.088	117	104	Bal.
HSLA	0.078	0.44	1.36	0.007	0.04	0.131	98	87	Bal.

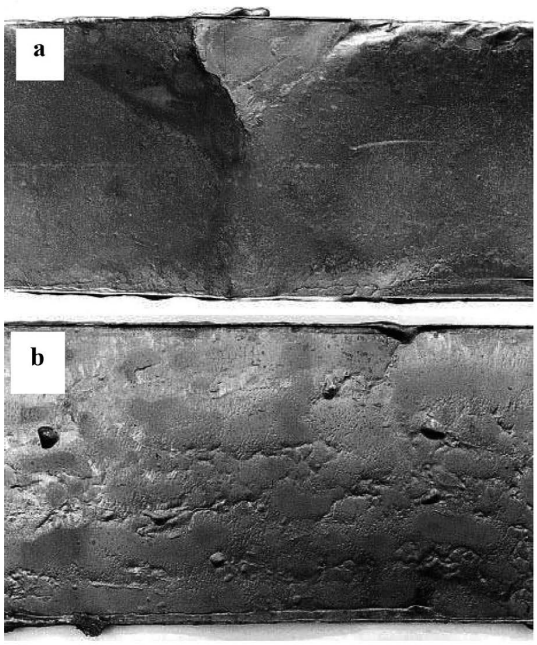

a triangle, crack, and lateral bead; *b* depressions, cracks, and bleeds

Fig. 7. Surface defects on 65 mm width strips.[23]

Table 2. Defects in as-cast steel strips.[23]

Defect	LC	LC+Ti	HSLA
Triangle defect	Strong	Slight	Slight
Bead	Frequent	None	None
Bleeds	Frequent	None	None
Edge defects	Strong	Slight	Slight
Depressions	Many	None	None
Surface cracks	Moderate	None	Moderate
Overall casting behaviour	Difficult	Good	Good

a without Ti; *b* with 0·088%Ti

Fig. 8. Effect of Ti on surface quality of twin-roll cast LC steel.[23]

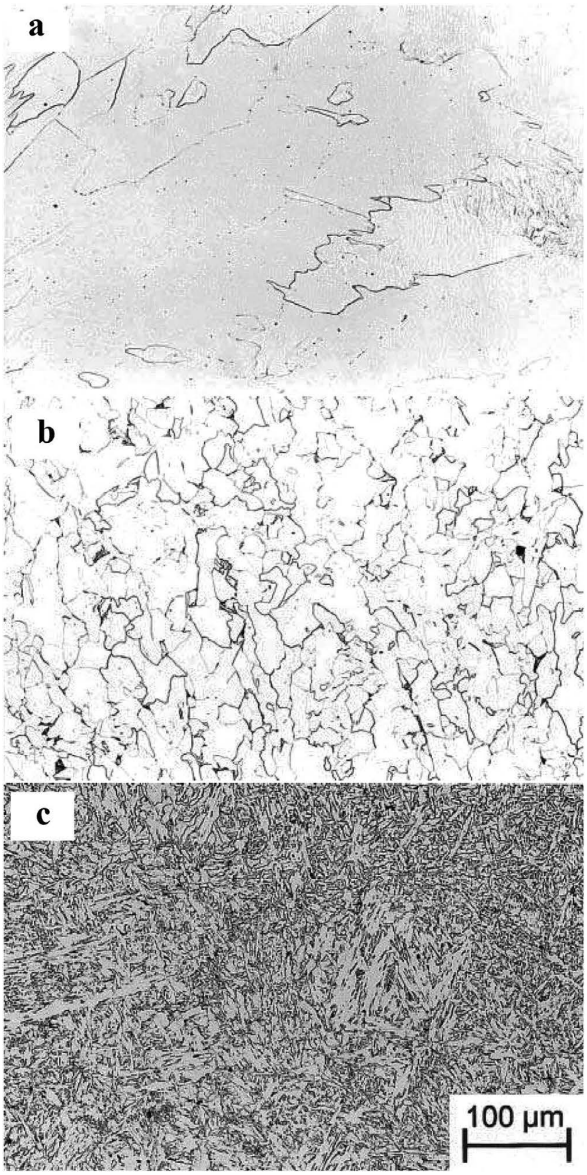

a LC; *b* LC + Ti; *c* HSLA

Fig. 9. Microstructures of the as-cast strips, air cooled.[23)]

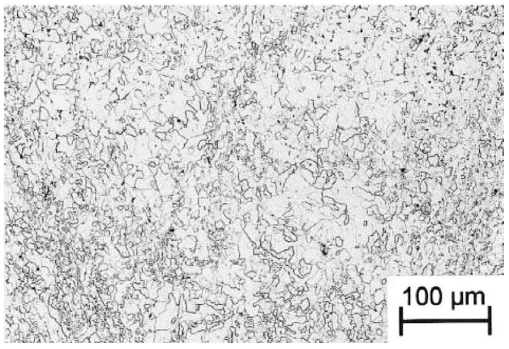

Fig. 10. Microstructure of LC+Ti steel strip after in-line hot-rolling, followed by air cooling.[23)]

structure has been modified considerably compared to Fig. 9(b). The ferrite grains are much finer and more uniform than in the as-cast and air cooled microstructure.

5.1.1.2. Effect of Annealing on TRC strip

In another research, Liu *et al.*[24)] investigated the differences in the mechanical properties between the as-cast and annealed low carbon steel strips with comparatively high contents of impurities in terms of the microstructural effects. The chemical composition of low carbon steel used in their study is given in **Table 3**.

Table 3. The chemical composition of cast steel strip, wt.%.[24)]

Steel	C	Si	Mn	P	S	Cu	Al_{tot}	O_{tot}	N	Fe
AC*/HA*	0.08	0.05	0.54	0.12	0.01	0.07	0.01	0.016	0.008	Bal.

(1) Al_{tot} and O_{tot} means total aluminum and total oxygen content in samples respectively.
(2) AC*: As-cast strip
(3) HA*: Treated strip

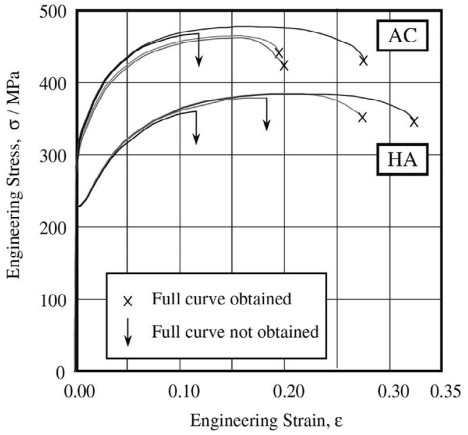

Fig. 11. Tensile test stress-strain curve of AC and HA strips.[24)]

The stress-strain behavior of AC and HA strips is shown in **Fig. 11**. The averages of yield strength and the tensile strength of the AC strip are 296 MPa and 468 MPa, respectively. These are noticeably higher than those of the HA strip; 228 MPa and 385 MPa, respectively. The value of TS-YS (work- hardening ability) is 170 MPa for the AC strip and 158 MPa for the HA strip. In fact, the AC strip in this study maintains the high work-hardening ability at higher stress levels compared to that of the HA strip.

The microstructures of AC and HA strips are shown in **Fig. 12**. Considering Fig. 12(a), the irregular polygonal ferrite and acicular ferrite is detected in AC strip. The high fraction of irregular polygonal ferrite in comparison with the acicular ferrite is attributed to the fine austenite grain size.[25)] Application of homogenization annealing (HA strip) results in conversion of acicular and irregular ferrites into more regular polygonal structure (Fig. 12(b)).

TEM images of AC strip are illustrated in **Fig. 13**. A lot of fine copper sulfides are observed with the mean size of ~ 15 nm. Considering Fig. 13(d), the main elements present in the EDS results are copper and sulfur. In the case of HA strip, the sulfides particles have grown and the number of them has decreased according to **Fig. 14**. The sulfides are about 100 ~ 800 nm with a mean size of about 200 nm. The second phase particles are believed to be mainly $Cu_{2-x}S$ type in both the AC and HA strip.

Liu *et al.*[24)] also calculated the yield strength of AC and HA strips as a function of volume fraction of copper sulfides particles. They observed that the increase in yield strength becomes larger by increasing the volume fraction of the particles and by decreasing the size of the particles (**Fig.**

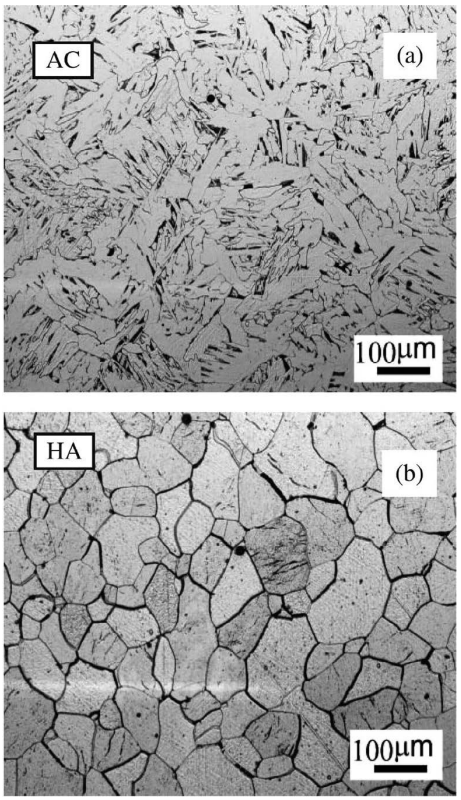

Fig. 12. Microstructure of (a) AC strip and (b) HA strip.[24]

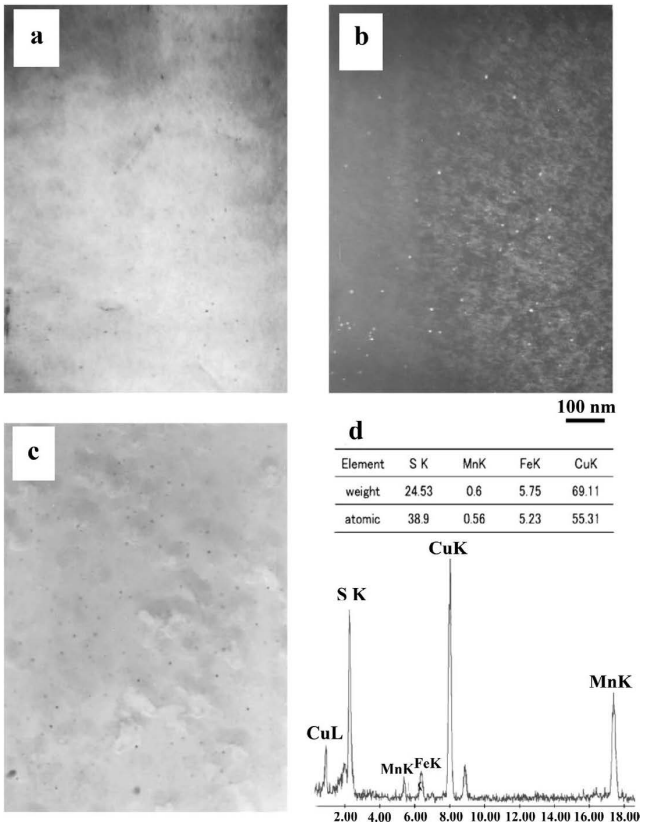

Fig. 13. Nano-scale copper containing sulfide particles (<20 nm) in AC strip. (a) bright field, thin foil; (b) dark field, thin foil; (c) bright field, extraction replica; (d) EDS.[24]

15). Consequently, the AC strip containing ~ 15 nm second phase particles represents higher yield strength compared to HA strip with ~ 200 nm second phase particles.

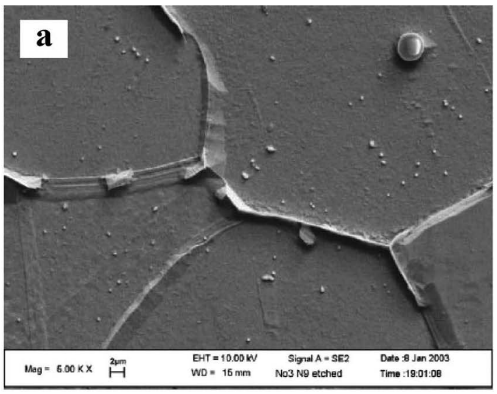

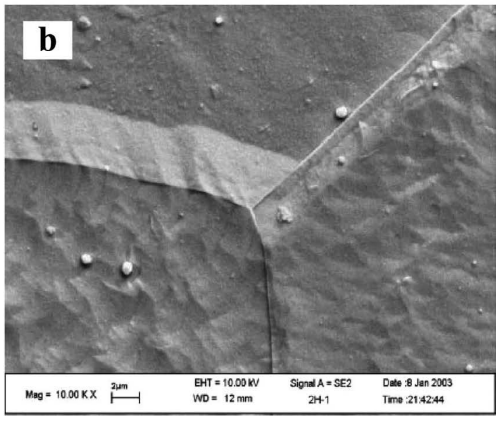

Fig. 14. Sulfide precipitates in HA strip (size: 100–800 nm).[24]

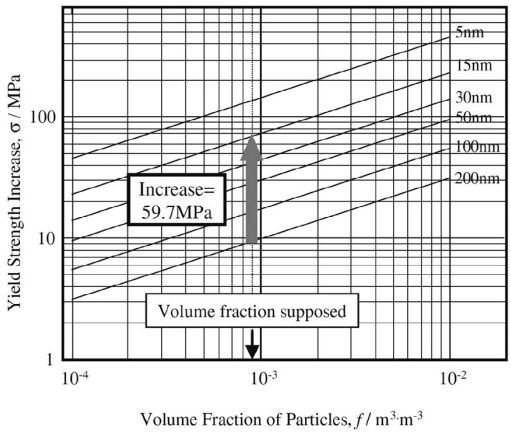

Fig. 15. The yield strength increase due to various volume fractions and sizes of particles in cast-strip steel.[24]

The hardness of AC and HA strip is sensitive to dislocation density as shown in **Fig. 16**. Cold-rolling increases the dislocation density and subsequently, both the hardness of AC and HA strip.

Additionally, the hardness values of AC strip are higher compared with that of HA strips. Thus the strain-hardening ability is much higher in the AC strip compared to that of the HA strip. The strain-hardening rate is obtained simply by the following equation:[24]

$$\frac{d\sigma}{d\varepsilon} = \frac{K_0}{2\sqrt{\varepsilon}} = 0.78KG\frac{b^{\frac{1}{2}}}{\varepsilon^{\frac{1}{2}}}\sqrt{\frac{f}{X}} \quad \text{..... (1)}$$

where σ is true stress, K is a constant of the order of 1, G is

the shear modulus of the matrix, b is the Burgers vector of the matrix dislocations, ε is the true strain, f is the volume fraction of particles, and X is the mean particle diameter.

In the study of Liu *et al.*,[24] particles volume fraction, f, was supposed to be almost similar for AC and HA strips and a square root of X for the AC strip was markedly smaller than that for the HA strip. This brings about a big difference in the strain-hardening between two low carbon steel strips (Eq. (1)).

5.1.1.3. Effect of Phosphorus

Hirata *et al.*[25] characterized the microstructures of 0.1 wt.% C steels with or without phosphorus addition produced by TRC. Three kinds of low carbon steels listed in **Table 4**, were used in this study.

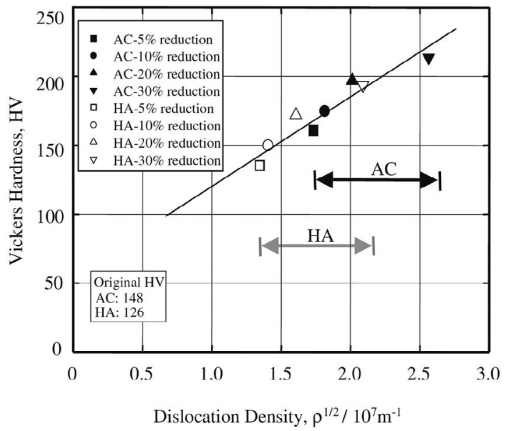

Fig. 16. Microhardness vs. dislocation density during deformation of AC and HA strips.[24]

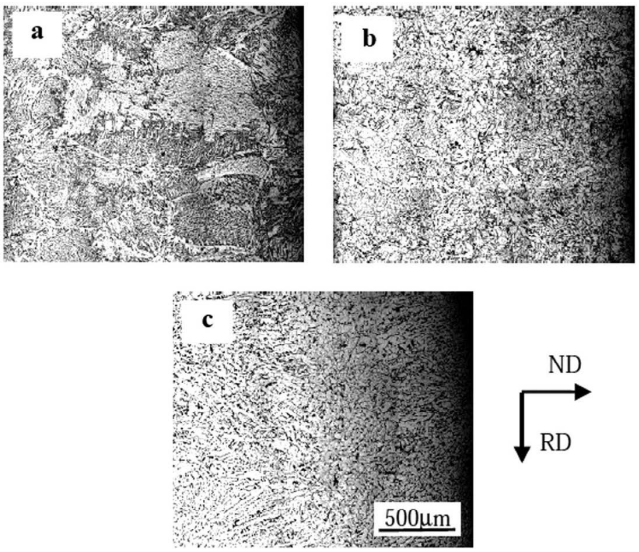

Fig. 17. Microstructure of low carbon cast strip steels in longitudinal section: (a) steel A, (b) steel B, and (c) steel C.[25]

Table 4. The chemical composition of low carbon cast strips.[25]

Material	Content (wt.%)				
	C	Si	Mn	P	S
A	0.11	1.17	0.62	0.014	0.014
B	0.09	0.17	0.62	0.082	0.016
C	0.11	0.16	0.67	0.197	0.014

Figure 17 shows the microstructure of low carbon cast strip steels. Steel A contains grain boundary and Widmanstatten ferrite, while steel C with high phosphorus content exhibits polygonal ferrite. In the case of steel B, both acicular and polygonal ferrite are obviously detected. In fact, the presence of different amount of phosphorus in A, B and C steels affects the nucleation and growth of ferrite grains changing the α-grain structure dramatically.

In 2007, Liu *et al.*[26] investigated the effect of phosphorus on sulfide precipitation, as well as the effect of sulfide on phosphorus micro-segregation in different twin-roll low carbon steel strips. They mentioned that the size of spherical sulfide particles becomes smaller in high phosphorus steel (HPS, 0.088 wt.% C and 0.081 wt.% P) sample compared to that in low phosphorus steel (LPS, 0.096 wt.% C and 0.013 wt.% P) sample. Besides, the composition of the spherical sulfides was mainly MnS in LPS sample while it was mainly $Cu_{2-x}S$ in HPS sample, indicating that phosphorus suppresses MnS precipitation and promotes $Cu_{2-x}S$ precipitation. **Figures 18** and **19** depict the sulfide particles within twin-roll HPS and LPS, correspondingly.

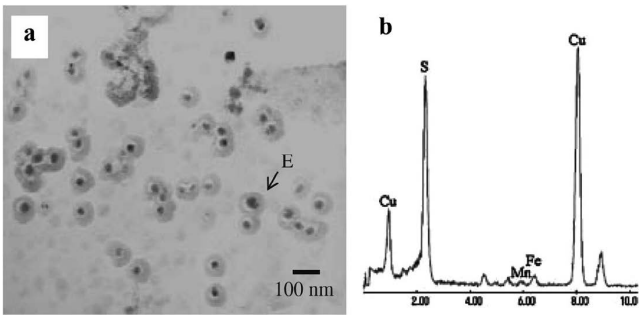

Fig. 18. Morphology and EDS of spherical sulfides in HPS sample. (a) TEM image and (b) EDS spectrum from extraction replica specimen.[26]

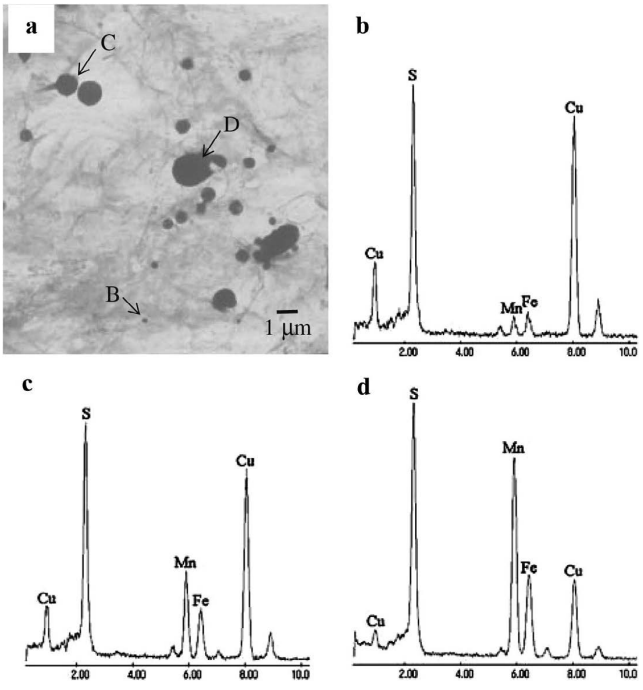

Fig. 19. Spherical sulfides in LPS sample. (a) Morphology; EDS of (b) Point B, (c) Point C, and (d) Point D.[26]

Considering Figs. 18 and 19, one can conclude that the HPS sample contains finer spherical sulfides compared to LPS sample. On the other hand, these researchers emphasized that the segregation degree of phosphorus in a sample containing sulfide particles is reduced if phosphorus has some solubility in sulfide particles and sulfide particles provide more interfaces for phosphorus to distribute. The area of these interfaces will greatly increase especially when the sulfide particles has a fine size (HPS sample).

5.1.2. Twin-roll Casting of Silicon Steels

5.1.2.1. Non Grain Oriented Electrical Steel

In the category of silicon steels, Fe–6.5 wt.% Si alloy is an appropriate candidate for application in the iron core of motors and generators working under high frequency conditions. Some drawbacks such as intrinsically limited ductility and the intercrystalline brittleness of Fe–6.5 wt.% Si alloy hinders the commercial application of this steel. Excessive rolling deformation during conventional rolling methods makes these techniques improper for production of Fe–6.5 wt.% Si thin sheets. Instead, the TRC technology which produces the near-net-shape as-cast strip directly from the melt offers significant potential advantages.

To benefit from positive solidification microstructure refining, grain boundary strengthening and inclusion modifying effects of the rare earth elements (REMs), Li *et al.*[27] investigated the as-cast strips of the Fe–6.5 wt.% Si alloy doped and undoped with Ce produced by TRC. To do so, two silicon steels, Fe–6.44Si–0.0036N–0.005S (1#) and Fe–6.48Si–0.023Ce–0.0048N–0.003S (2#) were employed in their study. **Figure 20** shows the as-cast EBSD microstructure of 1# and 2# silicon steel strips.

According to Fig. 20(a), the grain size of the 1# strip is very nonuniform along normal direction (ND), whereas in the case of 2# strip, the grain size distribution is much more uniform (Fig. 20(c)). In 1# strip, much finer equiaxed grains are near the surface due to the fact that rough surface of the casting rolls is considered as nucleation sites, while the internal part of the melt pool is far from the rough surface of the casting rolls inevitably suffers from insufficient nucleation sites. Considering Figs. 20(b) and 20(d), the length fraction of sub-grain boundaries for 2# strip is 40% higher than 1# strip. In fact, 2# strip has a higher solidification end point with respect to the roll nip point; consequently, 2# strip undergoes a larger rolling deformation during twin-roll casting leading to higher amount of sub-grain boundary fraction. **Figure 21** demonstrates coarse and hexagonal precipitates with an average diameter of about 2 μm in the grain interiors of the 2# strip. Regarding Fig. 21, these precipitates mainly consist of Ce, O and S suggesting the formation of Ce_2O_2S. The Ce_2O_2S particles act as nucleation sites enhancing heterogeneous nucleation.

The stress-strain behavior of 1# and 2# strips was also studied by these researchers. **Figure 22** illustrates the engineering stress–strain curves at 600°C. The 2# strip shows higher stress level in comparison with 1# strip because of grain refinement strengthening (Figs. 20(c), 20(d)). Additionally, the elongation for 2# strip was measured to be 56.8% which is significantly higher than 22.8% obtained for 1# strip.

In 2012, Zhang *et al.*[28] studied the influence of changing melt superheat on the solidification structure of 1.3%Si non-oriented electrical steel in the twin-roll strip casting process, and microstructure evolution during annealing of cold rolled sheet with different initial grain sizes. **Figure 23** illustrates the microstructure of as-cast strips achieved through various melt superheats. As indicated, the average grain size increases from 110 μm to 380 μm by increasing the melt superheats in the range of 20–60°C. At low melt superheat *i.e.* 20°C, high nucleation rate takes place during casting, causing the formation of fine equiaxed ferrite grains. Increasing the melt superheat up to 60°C, decreases nucleation rate, and consequently encourages formation of large irregular equiaxed ferrite grains and few columnar grains. In this case, very small amounts of fine ferrite grains are visible at the boundaries.

The microstructure of cold rolled and annealed cast-strip sheets with different melt superheats is shown in **Fig. 24**. As for 60°C melt superheat with larger as-cast grain size, larger grain size after cold rolling and annealing is obtainable.

5.1.2.2. Grain Oriented Electrical Steel

Wang *et al.*[29] produced a novel ultra-low carbon grain oriented silicon steel strip by TRC process. The chemical composition of tested steel in wt.% was 0.005C, 3.0Si, 0.18

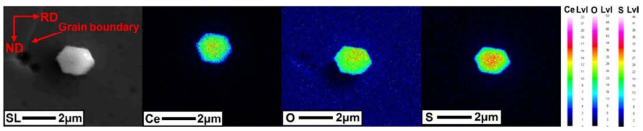

Fig. 21. Electron probe micro-analysis (EPMA) elemental mapping analyses of the grain-interior distributing precipitate in the 2# strip.[27] (Online version in color.)

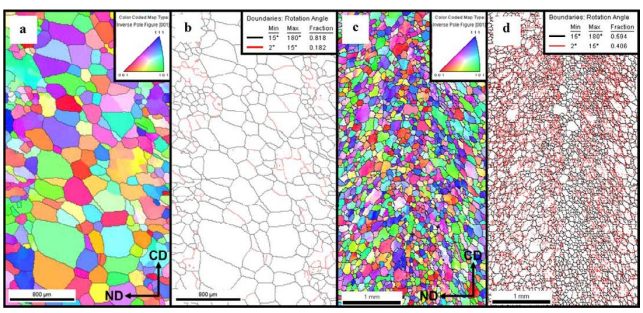

Fig. 20. Orientation image and the correspondingly grain-boundary maps of 1# (a, b) and 2# (c, d) strips.[27] (Online version in color.)

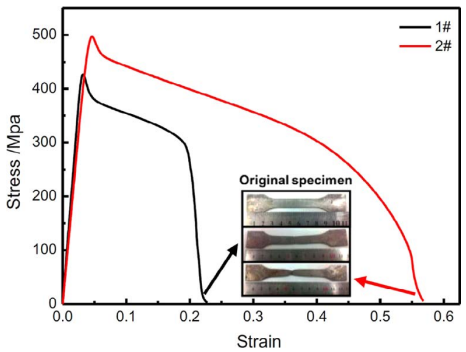

Fig. 22. Engineering stress–strain curves of the 1# and 2# tensile specimens tested at 600°C.[27] (Online version in color.)

Mn, 0.027Al, 0.029S, 0.0083N, and balance Fe. **Figure 25** indicates the SEM image of precipitates in the as-cast strip. As illustrated, the particles with an average size of ~ 100 nm are mostly distributed at grain boundaries and sub-grain boundaries. The EDS elemental mapping confirms that these particles are MnS, while the AlN particles remain in solution in the as-cast condition.

According to the equilibrium phase constituents diagram in ultra-low carbon silicon steels (**Fig. 26**), the starting precipitation temperature of MnS and AlN particles is 1 380°C and 1 280°C, respectively. It is worth noting that the plastic deformation and subsequent dislocation density induced by strip casting process are small. As a result, the MnS particles with higher precipitation temperature have a lot of nucleation sites such as grain boundaries and sub-grain boundaries. However, AlN particles with lower precipitation temperature have few appropriate nucleation sites. Moreover, the rapid solidification rate of TRC hinders the formation of AlN precipitates in the as-cast condition.

Figures 27(a)–27(c) shows the distribution of second phase particles in the intermediate annealed sheet after the different cold rolling reduction. After cold rolling, the deformed ferrite grains contain high dislocation density acting as nucleation sites for precipitation of AlN particles. Consequently, a large number of fine AlN particles is obtained during intermediate annealing.

The TEM micrograph and EDS (**Figs. 28**(a)–28(c)) confirms the presence of coarse and complex AlN+MnS precipitates (~ 80–120 nm) and fine AlN precipitates

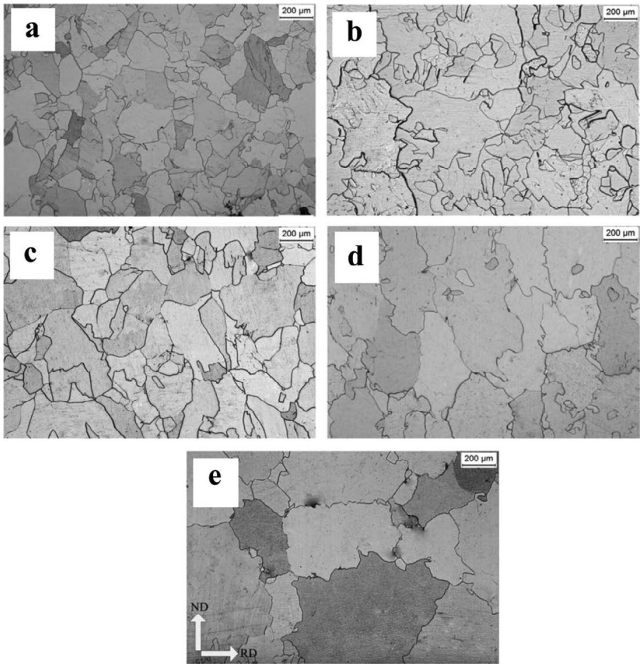

Fig. 23. Optical micrographs of 1.3%Si non-oriented electrical steel cast-strips at different melt superheats: (a) 20°C; (b) 30°C; (c) 40°C; (d) 50°C; and (e) 60°C.[28]

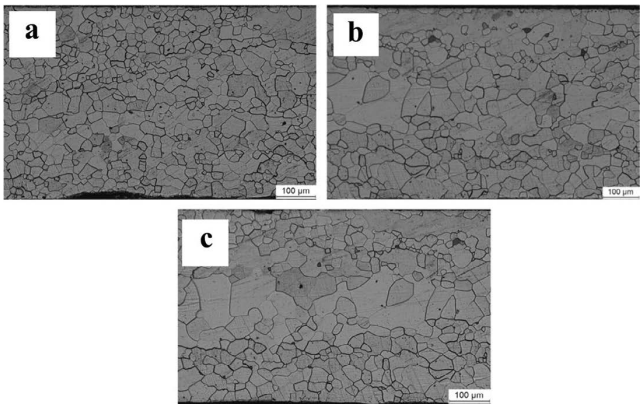

Fig. 24. Optical micrographs for the finally annealed sheets of cast-strips at different melt superheats: (a) 20°C; (b) 40°C; and (c) 60°C.[28]

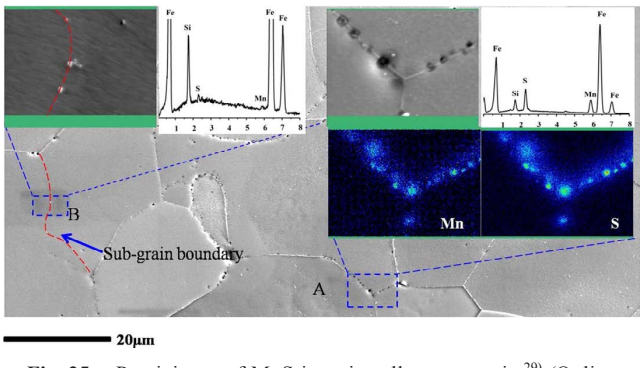

Fig. 25. Precipitates of MnS in twin-roll as-cast strip.[29] (Online version in color.)

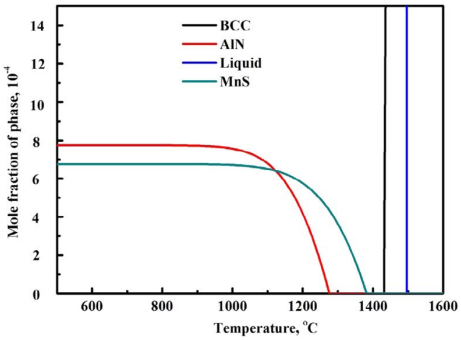

Fig. 26. Equilibrium phase constituents diagram in ultra-low carbon silicon steels.[29] (Online version in color.)

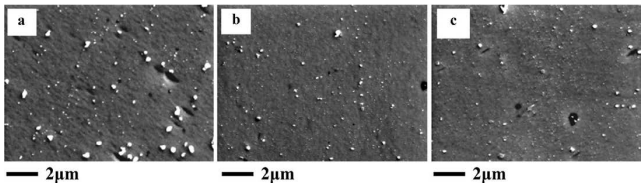

Fig. 27. SEM images of precipitates in the intermediate annealing sheets after different first cold rolling reductions: (a) 20%, (b) 40%, and (c) 60%.[29]

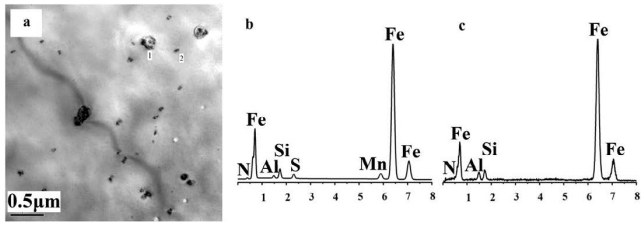

Fig. 28. (a) TEM image of precipitates in the intermediate annealed sheet after 20% cold rolling reduction, (b) EDS spectrum of particle 1, and (c) EDS spectrum of particle 2.[29]

(~ 20–50 nm). Higher cold rolling reduction can provide more nucleation sites for nucleation of particles, bringing about formation of more and finer AlN particles during intermediate annealing (as shown in Fig. 27). The AlN particles act as grain growth inhibitors suppressing grain growth mechanism during intermediate annealing treatment.[29] Additionally, these particles delay the crystal rotation during cold rolling such that part of the initial solidification texture remains in the cold rolled sheets.[30]

5.1.3. Twin-roll Casting of Stainless Steels

It has been reported in the literature that austenitic stainless steels such as AISI 304 are the most proper steel grades for direct strip casting.[31]

5.1.3.1. Microstructure

Mizoguchi and Miyazawa[32] studied the formation of solidification structure in twin roll casting process of 18Cr-8Ni stainless steel and stated that the solidified structure of the cast strip could be divided into two categories; one just included two columnar regions, whereas the other had an additional equiaxed region between the two columnar regions. Ji *et al.*[33] investigated the morphology of twin-rolled solidification structure of AISI 304 stainless steel including dendrites and grain boundaries using electron back-scattered diffraction (EBSD) analysis combined with the macro-etched method. The chemical composition of AISI 304 is indicated in **Table 5**.

Figure 29 shows a half of the microstructure of the twin-rolled strip along the casting direction. Considering Fig. 29, the microstructure includes columnar dendrite region, which transforms to equiaxed region at about 600–700 μm from the strip surface.

The EBSD analysis of columnar region is illustrated in **Fig. 30**(a). The columnar grains with the size of about 100 μm wide and 600 μm long are inclined to the casting direction like dendrite. Additionally, the grain morphology with small-angle grain boundaries (<15°), large-angle grain boundaries (>15°C) and some <111> twin boundaries are depicted in Fig. 30(b) with fine, thick and red lines, respectively.

Table 5. Chemical composition of the AISI 304 stainless steel (wt.%).[33]

C	Mn	P	S	Si	Ni	Cr	Cu	Mo	W	N	Fe
0.07	1.5	0.025	0.011	0.64	8.6	17.72	0.12	0.07	0.02	0.035	Bal.

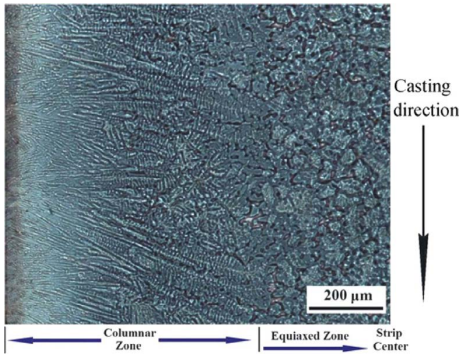

Fig. 29. Metallography of AISI 304 as-cast strip.[33] (Online version in color.)

As shown in Fig. 29, an equiaxed region with a thickness of about 1/4-1/3 of the total thickness is located between two columnar regions. The EBSD analysis of equiaxed grains along with its grain boundaries is presented in **Figs. 31**(a) and 31(b), correspondingly. The diameter of these inhomogeneous equiaxed grains varies between ~ 100–200 μm.

It should be noted that a transitional region with a thickness of ~ 100 μm is detected between columnar and equiaxed regions (**Fig. 32**(a)). The diameter of the equiaxed grains in the transitional region is considerably smaller than the equiaxed region varies in the range of 15–20 μm. Moreover, more small- angle grain boundaries are detected in the transitional region, as shown in Fig. 32(b). The amount of small-angle grain boundaries increases with the increase of distance from strip surface obtaining the maximum in the transitional region.

Wang *et al.*[34] also studied the microstructure of AISI 304 stainless steel produced by TRC. The 0.076C-1.332Mn-7.825Ni-18.06Cr stainless steel was used as the casting material in their research. **Figure 33** demonstrates the microstructure and XRD analyses of the twin-rolled cast stainless steel in two different positions: at surface and center section. According to XRD analysis, the microstructure of the cast strip includes two main phases, delta ferrite and

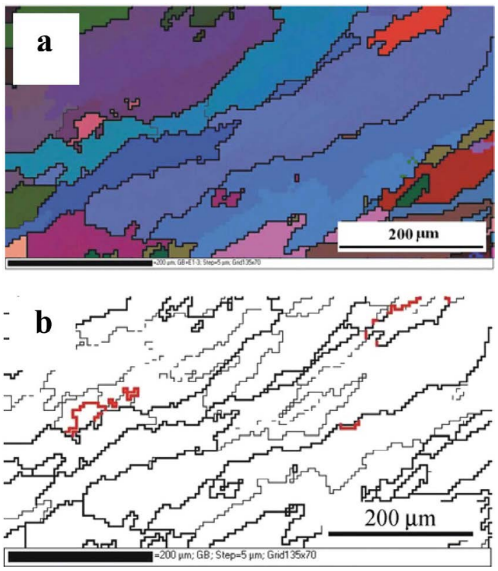

Fig. 30. (a) Morphology of columnar grains and (b) grain boundaries obtained by EBSD analysis.[33] (Online version in color.)

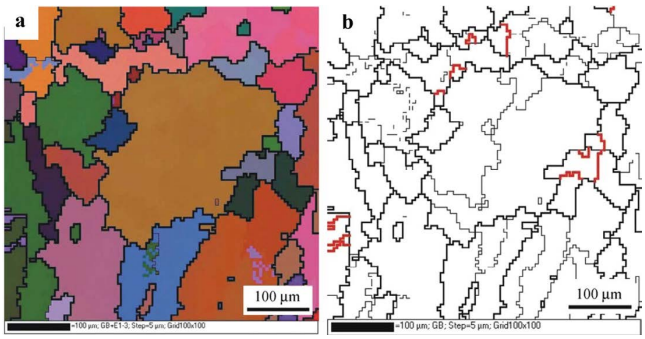

Fig. 31. (a) Morphology of equiaxed grains and (b) grain boundaries obtained by EBSD analysis.[33] (Online version in color.)

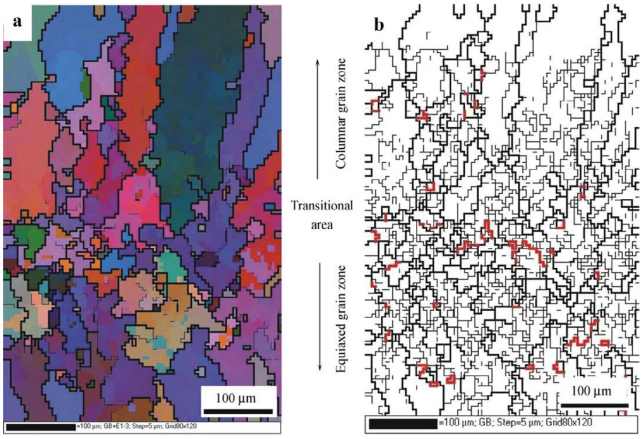

Fig. 32. Morphology of the transitional region from the columnar zone to equiaxed zone: (a) grain morphology; (b) grain boundary morphology.[33] (Online version in color.)

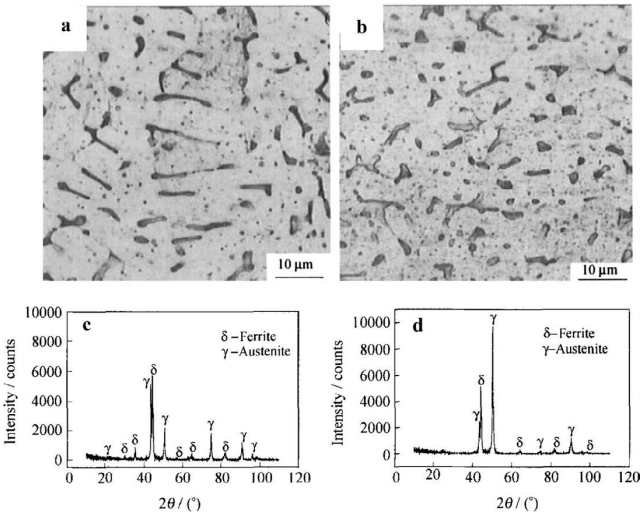

Fig. 33. Microstructures and XRD patterns of the AISI 304 twin-rolled cast sample in different sections: (a) microstructure at surface, (b) microstructure at center, (c) XRD pattern of surface, and (d) XRD pattern of center.[34]

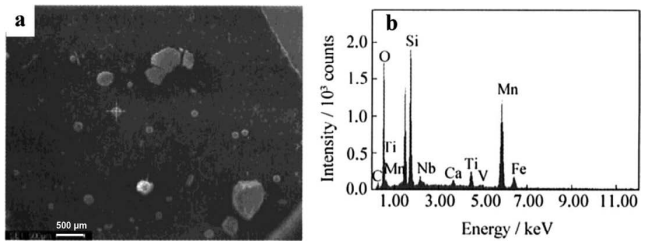

Fig. 34. SEM image and EDS pattern of the AISI 304 as-cast strip: (a) inclusions and (b) EDS pattern of inclusion.[34]

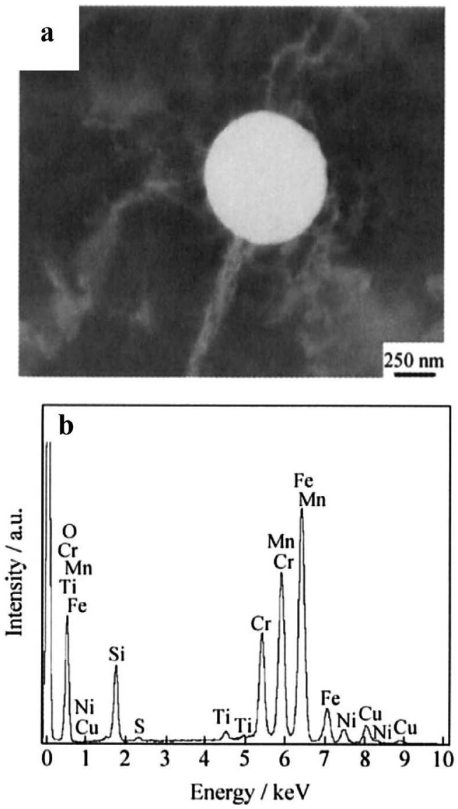

Fig. 35. TEM micrograph of the cast strip AISI 304 specimen showing (a) precipitates and (b) EDS of precipitates.[34]

austenite. Using graphical analysis method, the delta ferrite fraction is ~ 9.74 vol.% at the center and ~ 6.77 vol.% at the surface of the cast strip. The delta ferrite existence in the cast strip is mainly due to the fact that the Cr in the delta ferrite phase cannot fully diffuse into the austenite at the high solidification rate during the casting process. The morphology of delta ferrite in the cast strip is a vermicular type with a three-dimensional honeycomb network structure.[35]

5.1.3.2. Inclusions, Precipitates and Dislocations in as-cast Strip

SEM image and EDS pattern of as-cast strip is depicted in **Fig. 34**. According to the EDS pattern, it is suggested that the spherical inclusion in the casting thin strip might consist of oxides, such as, SiO_2 and MnO.

Furthermore, a high fraction of precipitates are also formed during TRC. **Figure 35** shows TEM micrograph of a spherical precipitate of 600–700 nm diameter. The precipitates are distributed in grain boundaries or within grains leading to a high density of dislocations piled up around the spherical precipitates. Dislocation strengthening is one of the mechanisms to improve the properties of materials. The relationship between dislocation strengthening and dislocation density is as follows:[36]

$$\sigma_d = M\alpha\mu b\rho^{1/2} \quad \text{..... (2)}$$

where σ_d, is the strength contribution due to dislocations, ρ is the dislocation density, M is the Taylor factor, α is a constant, μ is the shear modulus, and b is the Burger's vector. According to Eq. (2), the accumulation of dislocation around the precipitates and inclusions increases ρ causing the increase of σ_d.

5.1.3.3. Simulation of the Stress Field

An important phenomenon during TRC of stainless steels such as AISI 304 is crack initiation on the surface during the process.[37] The crack formation is mainly due to the temperature and stress fields. However, the stress field measurement by experiments is very difficult, since the stress on the surface could be released because of cracking and therefore residual stress field cannot be determined. As a result, simulation of the stress field seems to be an appropriate solution to overcome this challenge. Zhang *et al.*[38] simulated the stress field of 304 stainless steel during TRC process in which the casting speed, casting temperature,

roller radius and strip thickness, were 0.5 m s^{-1}, 1 500°C, 0.3 m and 2 mm, respectively. The result of simulation is indicated in **Fig. 36**.

According to Fig. 36, the thermal stress of the liquid region in melt cooling center is very small, even close to zero. The maximum tensile stress appears close to the roller nip at strip/roller interface, while the maximum compressive stress appears nearby the solidifying strip centerline.

5.1.4. Twin-roll Casting of High Manganese Steels

Recently, the automotive industries have focused on materials with high specific strength and work-hardening capabilities to achieve safety requirements for crash-relevant parts and to reduce greenhouse gas emissions. High-manganese twinning-induced plasticity (TWIP) steels meet these requirements due to their extraordinary combination of specific strength, high ductility and high work-hardening rate.[39,40] However, the wide use of these steels for industrial applications is limited due to their complex and expensive production processes. TRC is a promising alternative approach for fabrication of this class of materials.

5.1.4.1. Microstructure Analysis

Daamen *et al.*[41] studied the impact of Fe–29Mn–0.3C microstructure obtained through TRC on the resulting mechanical properties. **Figure 37** shows the microstructure of the specimen after TRC and subsequent inline hot-rolling. The microstructure of twin-rolled high manganese steel consists of a thin equiaxed center zone and two directionally solidified dendritic zones nucleated at the cooled casting rolls. The microstructure was altered significantly by additional thermo-mechanical post processing. **Figure 38** indicates the EBSD mapping after inline hot-rolling and cold-rolling/annealing treatments. According to Fig. 38, the inhomogeneous microstructure of as-cast and hot-rolled steel strip (Fig. 38(a)) converts to relatively homogeneous equiaxed microstructure after cold-rolling and annealing at 900°C and 1 150°C for 30 min (Figs. 38(b) and 38(c), respectively). Additionally, increasing the temperature of annealing treatment results in growth of equiaxed grains.

The results of the uniaxial tensile tests are displayed in **Fig. 39**. According to Fig. 39(a), the yield strength and elongation of as-cast and cold-rolled/annealed steel is in the range of 220–240 MPa and 60–65%, correspondingly. As for hot-rolled specimen, the yield stress reveals a slight increase (310 MPa) but a reduced uniform elongation of 53.2% due to 20% thickness reduction. Moreover, the work hardening rate of the cold-rolled/annealed specimen is also improved compared to the as-cast and the hot-rolled specimens (see Fig. 39(b)). The authors claimed that the rise of deformation twin fraction along with reduced grain size after recrystallization (Fig. 38(b)) increases the work-hardening rate of cold-rolled/annealed steel strip.[41]

In another study, Liu *et al.*[42] developed a high manganese

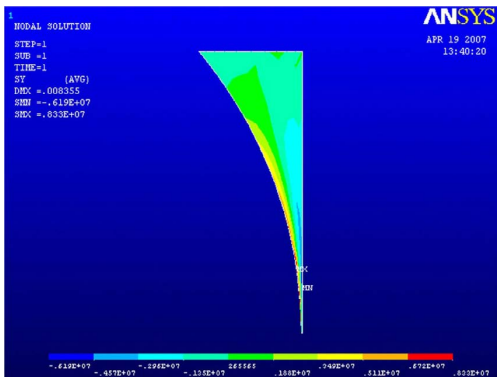

Fig. 36. Stress field of 304 stainless steel strip above the exit.[38] (Online version in color.)

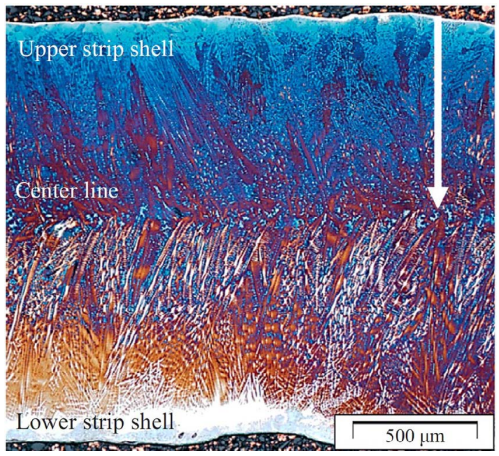

Fig. 37. Optical micrograph of Fe–29Mn–0.3C after strip casting and inline hot-rolling.[41] (Online version in color.)

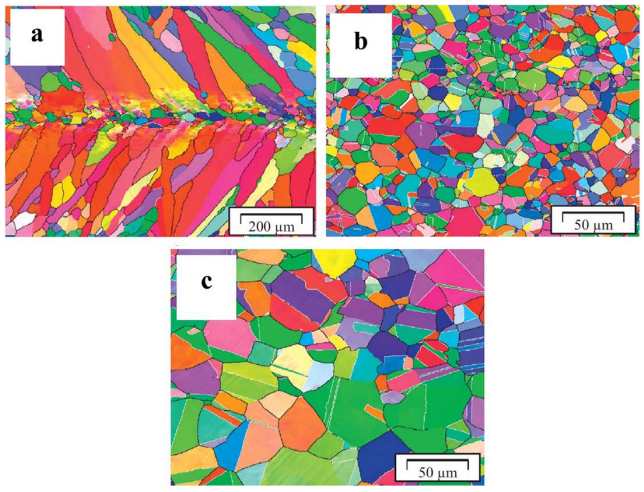

Fig. 38. EBSD mapping of Fe–29Mn–0.3C steel (a) after TRC and in-line hot-rolling, (b) after cold- rolling and annealing at 900°C and (c) after cold- rolling and annealing at 1 150°C , for 30 min.[41] (Online version in color.)

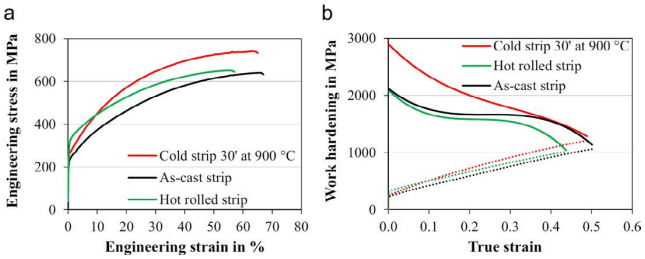

Fig. 39. (a) Engineering stress–strain curves and (b) trues tress–strain curves (dashed lines) and work-hardening rate–true strain curves (solid lines) of the high manganese steel after strip casting, hot-rolling, and cold- rolling and annealing at 900°C.[41] (Online version in color.)

austenitic stainless steel of Fe-25Mn-22Cr-2Si-0.7N using TRC and investigated its microstructure and mechanical properties in the as-cast and solution treatment at 1 050°C for 30 min conditions.

Figure 40 shows the optical and TEM micrographs of Fe-25Mn-22Cr-2Si-0.7N as-cast strip. According to Fig. 40(a), the primary dendrite arm spacing (PDAS) and secondary dendrite arm spacing (SDAS) are estimated to be ~ 10 μm and ~ 5–6 μm, respectively. The small SDAS is due to the TRCrapid cooling rate of austenitic stainless steel (14 000 K/s). The TEM micrograph emphasizes the formation of dislocations within the grains during strip casting.

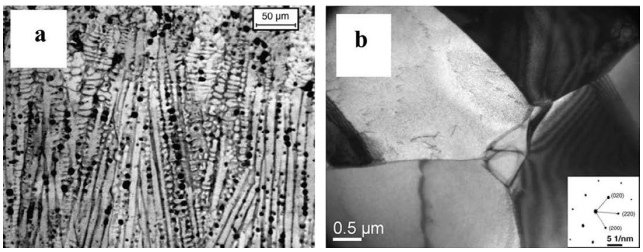

Fig. 40. (a) Optical image of solidification structure, and (b) TEM micrograph of n as-cast strip of high manganese steel.[42]

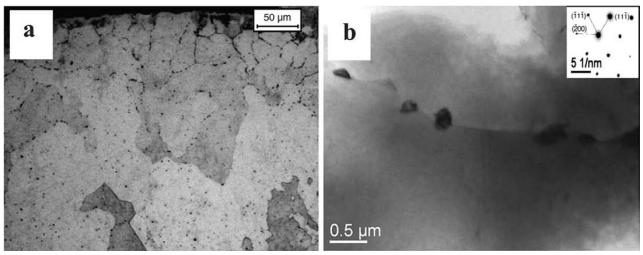

Fig. 41. (a) Optical and (b) TEM micrographs of steel strip after solid solution treatment at 1 050°C for 30 min.[42]

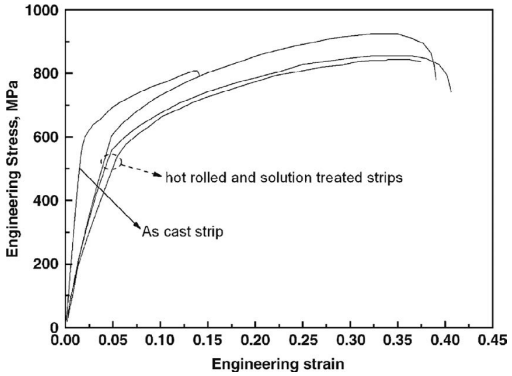

Fig. 42. Engineering stress-strain curves of the as-cast and hot rolled/solution treated strips.[42]

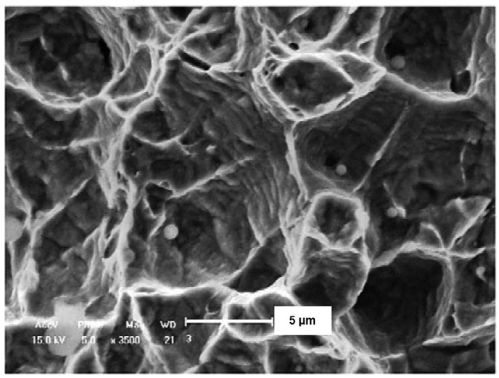

Fig. 43. Fracture surface of the as-cast strip after the tensile testing at a speed of 10 mm/min.[42]

After solution treatment at 1 050°C for 30 min, the austenite grains near the strip surface are ~ 25 μm, whereas the grains far from the surface grow up to ~ 100 μm (**Fig. 41**(a)). Additionally, some small precipitates are formed at the grain boundaries and smaller number of dislocations is detected within the grains (Fig. 41(b)).

5.1.4.2. Mechanical Behavior and Fracture Morphology

The engineering stress-strain curves of the as-cast and solution treated high manganese steel strips is shown in **Fig. 42**. It can be observed that the as-cast strip has acceptable yield strength of ~ 500 MPa. Moreover, the elastic modulus of the as-cast strip is higher than that of solution treated samples by an order of magnitude.

Considering Figs. 40 and 41, the high dislocation density of as-cast strip, induced by rapid solidification rate during TRC, significantly decreases after solution treatment at 1 050°C. Moreover, formation of precipitates at the grain boundaries (Fig. 41(b)) results in consumption of interstitial atoms such as C and N and subsequent reduction of lattice distortion. As a consequence, both reduction of dislocation density and formation of precipitates bring about lower elastic modulus after solution treatment at 1 050°C for 30 min (Fig. 42).[42]

The fracture surface of as-cast strip after tensile test is illustrated in **Fig. 43**. The ductile fracture as evidenced by dimple morphology initiated from second phase particles. In fact, no protective atmosphere is used during TRC causing the formation of oxides in the as-cast strip. These oxide particles deteriorate the ductility by generating micro-voids as shown in Fig. 43.

6. Conclusions

Sir Henry Bessemer's idea in 1857 was start of lots of efforts have been done to date toward commercialization of DSC, especially TRC technique. Nowadays, TRC is widely used to produce different categories of steels. This overview provided a comprehensive understanding of principles of TRC and its application for production of low carbon (LC) steels, silicon steels, stainless steels as well as high manganese steels. The summary is as follows:

(1) The addition of small amount of Ti to ordinary LC steels significantly decreases the casting defects during TRC process. As well, titanium addition decreases the average grain size of irregular ferrite and some signs of dark pearlite grains become visible in the microstructure.

(2) The as-cast low carbon (AC) strip exhibits high work-hardening ability at higher stress levels compared to that of the treated low carbon (HA) strip. Additionally, AC strip containing ~ 15 nm second phase particles shows higher yield strength compared to HA strip with ~ 200 nm second phase particles. The smaller mean diameter of copper containing sulfide particles in AC strip causes higher strain-hardening with respect to HA strip.

(3) Using Ce as dopant in silicon steels (6.5 wt.% Si) results in the formation of Ce_2O_2S particles which act as nucleation sites enhancing heterogeneous nucleation and

the subsequent grain refinement strengthening during TRC.

(4) Increasing the melt superheat from 20°C to 60°C during TRC of silicon steels (1.3 wt.% Si) changes the morphology of fine equiaxed ferrite to irregular equiaxed and columnar ferrite.

(5) The microstructure of AISI 304 stainless steel produced by TRC consists of two columnar regions and an equiaxed region so that a transitional region is located between the columnar and equiaxed region. The transitional region includes much finer equiaxed grains and subsequently more small-angle grain boundaries compared to equiaxed region.

(6) The spherical inclusions in twin-rolled AISI 304 stainless steel (0.076C-1.332Mn-7.825Ni-18.06Cr) are mainly SiO_2 and MnO. The accumulation of dislocations around these inclusions and precipitates increases the dislocation strengthening.

(7) The inhomogeneous microstructure of twin-rolled high manganese steel in as-cast and hot-rolled condition converts to relatively homogeneous equiaxed microstructure after cold-rolling and annealing at 900°C and 1 150°C for 30 min.

(8) The fracture surface of twin-rolled high manganese steel shows the ductile fracture as evidenced by dimple morphology initiated from oxide particles formed in the as-cast strip during TRC process.

REFERENCES

1) M. Ghosh, N. Sen, A. Paul, A. K. Ray, R. Sau and S. Chakraborty: *Ironmaking Steelmaking*, **27** (2000), 310.
2) E. E. M. Luiten and K. Blok: *Energy Policy*, **31** (2003), 1339.
3) S. Ge, M. Isac and R. I. L. Guthrie: *ISIJ Int.*, **52** (2012), 2109.
4) Z. Xia, Y. Kang and Q. Wang: *J. Magn. Magn. Mater.*, **320** (2008), 3229.
5) S. Ge, M. Isac and R. I. L. Guthrie: *ISIJ Int.*, **53** (2013), 729.
6) Castrip LLC: (2000), http://www.castrip.com, (accessed 2016-05-10).
7) D. Raabe, R. Degenhardt, R. Sellger, W. Klos, M. Sachtleber and L. Ernenputsch: *Steel Res. Int.*, **79** (2008), 440.
8) D. Raabe: *Metall. Mater. Trans. A*, **26** (1995), 991.
9) D. Raabe: *Mater. Sci. Technol.*, **11** (1995), 461.
10) W. Blejde, F. Fisher, M. Schueren and G. McQuillis: Proc. 10th Int. Conf. on Steel Rolling, Chinese Society for Metals, Beijing, (2010).
11) E. E. M. Luiten: PhD Thesis, Utrecht University, (2001), http://dspace.library.uu.nl/bitstream/handle/1874/746/full.pdf, (accessed 2001-09-13).
12) C. W. Zang and C. C. Ta: *Acta Phys. Sin.*, **9** (1953), 57.
13) N. Zapuskalov: *ISIJ Int.*, **43** (2003), 1115.
14) M. Ferry: Direct Strip Casting of Metals and Alloys Processing, Microstructure and Properties, Woodhead Publishing and Maney Publishing, Cambridge, England, (2006), 96.
15) H. O. Fitzel, P. L. Steger, A. Gstottenmayr and G. P. Danninger: *Steel Times*, **224** (1996), 256.
16) Castrip LLC: (2006), http://www.castrip.com, (accessed 2016-05-02).
17) C. R. Taylor: *Metall. Trans. B*, **6** (1975), 359.
18) C. Hendricks: *Metall. Plant Technol. Int.*, **18** (1995), 42.
19) P. Campbell, W. Blejde, R. Mahapatra and R. Wechsler: *Metallurgist*, **48** (2004), 507.
20) A. W. Cramb: *Iron Steelmaker*, **15** (1988), 45.
21) P. A. Manohar, M. Ferry and A. Hunter: *Mater. Forum*, **24** (2000), 19.
22) H. K. Moon, D. K. Choo, T. Kang and K. S. Kim: Proc. 60th Electric Furnace Conf., Iron & Steel Society, Warrendale, PA, (2002), 499.
23) A. Girgensohn, A. R. Buchner and K. H. Tacke: *Ironmaking Steelmaking*, **27** (2000), 317.
24) Z. Liu, Y. Kobayashi and K. Nagai: *Mater. Trans.*, **45** (2004), 479.
25) K. Hirata, O. Umezawa and K. Nagai: *Mater. Trans.*, **43** (2002), 305.
26) Z. Liu, Y. Kobayashi, M. Kuwabara and K. Nagai: *Mater. Trans.*, **48** (2007), 3079.
27) H. Z. Li, H. T. Liu, X. L. Wang, G. M. Cao, C. G. Li, Z. Y. Liu and G. D. Wang: *Mater. Lett.*, **165** (2016), 5.
28) Y. Zhang, Y. Xu, H. Liu, C. Li, G. Cao, Z. Liu and G. Wang: *J. Magn. Magn. Mater.*, **324** (2012), 3328.
29) Y. X. Zhang, X. Lu, F. Fang, Y. B. Xu, G. M. Cao, C. G. Li, R. D. K. Misra and G. D. Wang: *J. Magn. Magn. Mater.*, **419** (2016), 225.
30) Y. Wang, Y. B. Xu, Y. X. Zhang, F. Fang, X. Lu, R. D. K. Misra and G. D. Wang: *Mater. Charact.*, **107** (2015), 79.
31) T. Yamauchi, T. Nakanori and M. Hasegawa: *Trans Iron Steel Inst. Jpn.*, **28** (1988), 23.
32) T. Mizoguchi and K. I. Miyazawa: *ISIJ Int.*, **35** (1995), 771.
33) C. Ji, J. Zhang, F. Huang, X. Wang, Y. Fang and Y. Yu: *J. Univ. Sci. Technol. B.*, **15** (2008), 678.
34) Z. Wang, Y. Fang, J. Qi, Y. Zhang, Y. Yu and J. Wu: *J. Univ. Sci. Technol. B.*, **14** (2007), 420.
35) S. H. Kim, H. K. Moon, T. Kang and C. S. Lee: *Mater. Sci. Eng. A*, **356** (2003), 390.
36) D. A. Hughes: *Mater. Sci. Eng. A*, **319**–**321** (2001), 46.
37) R. Kopp, F. Hagemann, L. Hentschel, J. Schmitz and D. Senk: *J. Mater. Process. Technol.*, **80**–**81** (1998), 458.
38) P. Zhang, Y. Zhang, L. Liu, X. Ren, Y. Zhang, Y. Fang and Q. Yang: *Comp. Mater Sci.*, **52** (2012), 61.
39) B. C. De Cooman, K. G. Chin and J. Kim: New Trends and Developments in Automotive System Engineering, ed. by M. Chiaberge, InTech, Rijeka, Croatia, (2012), 101.
40) O. Kwon, K. Y. Lee, G. S. Kim and K. G. Chin: *Mater. Sci. Forum*, **638**–**642** (2010), 136.
41) M. Daamen, C. Haase, J. Dierdorf, D. A. Molodov and G. Hirt: *Mater. Sci. Eng. A*, **627** (2015), 72.
42) Z. Y. Liu, Z. S. Lin, S. H. Wang, Y. Q. Qiu, X. H. Liu and G. D. Wang: *Mater. Charact.*, **58** (2007), 974.